IROS '94

Volume 1

Proceedings of the
IEEE/RSJ/GI International Conference on

Intelligent Robots and Systems

Advanced Robotic Systems and the Real World

September 12 - 16, 1994
Federal Armed Forces University Munich
Germany

SPATIAL CHARACTERISTICS OF HUMAN HAND IMPEDANCE
IN MULTI-JOINT ARM MOVEMENTS

Toshio TSUJI[1], Kazuhiro GOTO[1], Masamitsu MORITANI[1],
Makoto KANEKO[1] and Pietro MORASSO[2]

[1]Computer Science and Systems Engineering, Hiroshima University
Kagamiyama 1-chome, Higashi-Hiroshima, 724 Japan
E-mail: tsuji@huis.hiroshima-u.ac.jp

[2]DIST - University of Genova, Laboratory for Integrated Advanced Robotics (LIRA - Lab)
Via Opera Pia 11A, I16145 Genova, Italy

Abstract

The present paper examines spatial characteristics of human hand impedance in multi-joint arm movements. While a subject maintains a hand location, small external disturbance to his hand is applied by a manipulandum. Time changes of the hand displacements and forces caused by the disturbance are measured, and the hand impedance is estimated using a second-order linear model. The estimated hand impedance in different subjects and hand locations are summarized as follows: 1) spatial variations of the estimated hand impedance ellipses approximately agree with the experimental results of other researchers (Mussa-Ivaldi et al., 1985; Dolan et al., 1993), 2) the human hand inertia characteristics can be explained from basic biomechanics of the passive inertial effects, 3) the grip force of the subject increases the size of the stiffness and viscosity ellipses, and 4) spatial features of the orientation and the shape characteristics of the stiffness and viscosity ellipses are mostly explained from the kinematics point of view of the human arm.

1. Introduction

Generally speaking, robots have been developed so far in order to execute tasks instead of human workers. In contrast, design and control of a robot system which performs tasks in cooperation with human operators have become an area of great interest in recent years. In order to develop such control systems with man-machine interactions, the knowledge of mechanical characteristics of the human movements as well as the robot is required.

Impedance is often used to describe the mechanical characteristics of the human arm [1]-[3]. Kazerooni [2] and Kosuge et al. [3] modeled man-machine interaction using the experimentally estimated human arm impedance to design the control system. In their estimations, however, several important aspects on human arm impedance such as configuration dependency, spatial properties and effects of muscle contraction level were ignored.

Understanding the impedance characteristics of the human arm has lately attracted considerable attention not only in the robotics field, but rather, in the biological field. For the multi-joint arm movements, Mussa-Ivaldi et al. [4] developed an experimental method to estimate human hand stiffness during maintaining posture. The experimental results indicated that the stiffness ellipses at any hand location tended to have the orientations toward the shoulder of the subject. Flash and Mussa-Ivaldi [5] showed that these spatial variations of the hand stiffness could be explained by a covariation between the shoulder stiffness and the stiffness component provided by two-joint muscles. Also, Dolan et al. [6] extended the experimental method developed in [4] to include measurement of dynamic components such as viscosity and inertia as well as stiffness. They showed that the viscosity ellipses tended to have the similar orientation as the corresponding stiffness ellipses. Their estimated results of the hand inertia, however, considerably differed from the calculated values using a two-joint mechanical model of the human subject and varied depending on the filtering method applied to the measured signals. Also, no appropriate explanation has been made yet for the reason why those spatial features of human hand impedance were

423

observed.

In the present paper, we estimate the human hand impedance in the multi-joint arm movements and check the validity of the estimated hand inertia by using the mechanical model of the human arm. Then, a graphical representation of the estimated hand impedance as an ellipse is used, and three components characterizing the spatial feature of the ellipses corresponding to hand stiffness and viscosity, i.e., size, orientation and shape, are examined. The characteristics of the hand viscoelasticity may be affected by kinematic property of the human arm, motor control signals from central nervous system (CNS), and individual properties of each muscle [4], [5]. This paper concentrates on the first factor, that is kinematic property of the human arm, and analyzes to what extent this factor can explain the spatial characteristics of the human hand stiffness and viscosity during maintaining the posture.

2. Methods [7]

2.1 Hand Impedance Model

In order to estimate the hand impedance, the hand of the subject is displaced from an equilibrium by means of a small disturbance with short duration (see **Fig.1**). The hand inertia, viscosity, stiffness and virtual equilibrium point are assumed to be constant after the onset of the disturbance. Then, we can limit ourselves to a time independent second order linear impedance model of the hand dynamics:

$$M d\ddot{X}(t) + B d\dot{X}(t) + K dX(t) = -dF(t), \quad (1)$$

where $dX(t) \equiv X(t)-X(t_0) \in \Re^l$ is the hand displacement vector, $dF(t) \equiv F(t)-F(t_0) \in \Re^l$ is the hand force exerted from the hand to the environment and t_0 denotes the onset time of the disturbance. Also, M, B and $K \in \Re^{l \times l}$ represent hand inertia, viscosity and stiffness matrices, respectively, and l is the number of degrees of freedom of the task space.

In equation (1), M, B and K are unknown parameters and the other variables either are direct measurements ($X(t)$ and $F(t)$) or can be derived by numerical methods. To estimate the impedance, we applied the standard least square procedure not to equation (1) but to the following one, obtained by integrating twice over time,

$$M dX(t) + B \int_0^{t_f} dX(t)dt + K \int\int_0^{t_f} dX(t)dt^2 = -\int\int_0^{t_f} dF(t)dt^2, \quad (2)$$

because integration is numerically a more robust operator than differentiation. Note that t_f denotes the length of the data observation window.
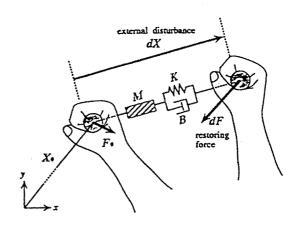

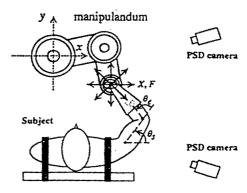Fig.1 Description of hand impedance for small motions around an equilibrium posture

Fig.2 Subject and manipulandum

2.2 Experiments

Figure 2 shows experimental apparatus for hand impedance estimation. A two-joint planar direct drive robot was used as a manipulandum to apply the external displacements to the hand of the subject. The force vector between the hand and the handle was measured by a force sensor attached to the robot handle (resolution: 0.05 N for both x and y axes). The arm posture of the subject was measured by a stereo PSD camera system that was able to compute a 3D arm posture from detected positions of four LED targets attached to shoulder, elbow and wrist joints of the subject and the robot handle. The data sampling intervals were 1 ms for hand forces and positions, and 10 ms for 3D arm postures.

The subject took a seat in the front of the robot (see Fig.2) similarly to the experimental method developed by Mussa-Ivaldi et al. [4]. The shoulder of the subject was restrained by a belt to the chair back and the elbow of the right arm was supported in the horizontal plane by a chain
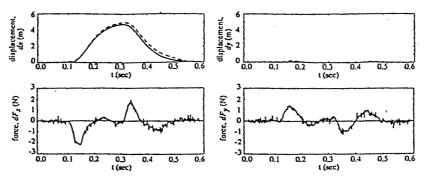
424

Fig.3 Example of measured hand displacement $dX(t)$ and force $dF(t)$ during maintaining posture, where the disturbance was applied along the direction of the x axis

attached to the ceiling. The wrist and the hand were fixed by a molded plastic cast (mass: 0.164 kg) tightly attached to the robot handle in order to eliminate the need of a voluntary grasping action. Moreover, for avoiding voluntary responses of the subject evoked by visual feedback, the robot handle and subject's arm were hidden by a cover in such a way that the subject couldn't see the robot and arm movements.

Firstly, the subject was asked to relax his arm in order to have a low value of the initial hand force to the handle, and to keep his hand at the initial position. Then an external disturbance was applied to his hand by the robot. In order to eliminate any significant influence of voluntary responses of the subject on the performed measurements, the disturbance pattern which returns to the initial position in a short period and has the amplitude for about 5 mm was used (see **Fig.3**). The onset time of the disturbance and its direction among eight possible ones (see Fig.2) were chosen in a random way. Then the hand displacements, $dX(t)$, and hand force, $dF(t)$, were measured, and the hand impedance parameter, M, B, K, were estimated for a set of data corresponding to eight disturbances with different directions.

3. Estimated Human Hand Impedance

Four male subjects, 21-23 years old, performed the required task. The number of the different hand locations used in the experiments was twenty for one subject and eleven for others. Fig.3 shows an example of the measured hand displacement, $dX(t)$, and force $dF(t)$, where the disturbance is applied along the direction of x axis. The measured time history of the displacement, $dX(t)$, (the solid lines) well agrees with the predicted value (the dashed lines) computed by solving (1) with estimated impedance, M, B, K, and measured force $dF(t)$.

The estimated inertia matrices and viscosity matrices are approximately symmetrical. The symmetrical components of the estimated impedance matrices are used in the following discussions by extracting the corresponding eigenvectors and eigenvalues and displaying them with an elliptic plot.

3.1 Hand Inertia

Figure 4 shows inertia ellipses corresponding to the mean values of the estimated inertia of a subject. The inertia ellipse graphically represents the locus of the hand force vectors determined by an input disturbance consisting of an acceleration vector of unit length (1 m/s^2) rotated in all possible directions [4]. The four subjects, as might be expected from the similarity of their kinematic structure, exhibit a similar pattern of hand inertia variation.
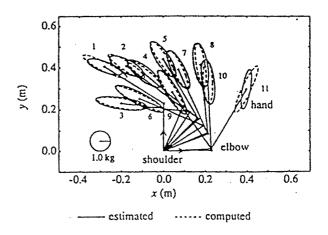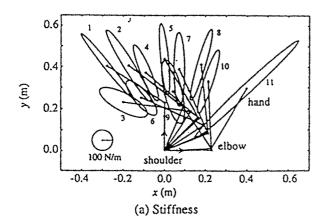

——— estimated   ······ computed

Fig.4 Estimated hand inertia ellipses

425

Table 1 Link parameters of an arm model used in calculations of the equivalent hand inertia

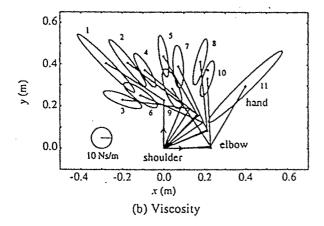| Link	Length [m]	Mass [kg]	Center of mass [m]	Inertia [$\times 10^{-3}$ kgm^2]
upper arm	0.23	1.82	0.10028	9.982
forearm + hand	0.33	1.43	0.15840	34.108

(a) Stiffness

(b) Viscosity

Fig.5 Estimated hand viscoelastic ellipses

We also computed the inertia matrices from the motion equation of the two-link arm model based on anatomic measurements on the link lengths of each subject and estimated values of the corresponding masses and moments of inertia using the method of Winter [8]. The estimated link parameters are listed in **Table 1** and the dashed ellipses in Fig.4 show the computed results. Although the differences between the estimated and computed ellipses could be analyzed in details as regards the

measurement and / or approximation errors, it can be seen that in qualitative terms, the human hand inertia characteristics in multi-joint movements can be explained from basic biomechanics.

3.2 Hand Viscoelasticity

Figure 5 (a) shows stiffness ellipses representing the symmetrical components of the mean values of the estimated stiffness matrices, which are corresponding to the inertia ellipses in Fig.4. The stiffness ellipse graphically represents the locus of the hand force vectors determined by an input disturbance consisting of a displacement vector of unit length (1 m) rotated in all possible directions [4].

Human hand stiffness characteristics during maintaining posture were analyzed for the first time by Mussa-Ivaldi et al. [4]. In agreement with their result, our data can be characterized as follows: 1) the major axes of the stiffness ellipses tend to be oriented toward the shoulder of the subject, 2) the ellipses become more elongated as the hand location approaches the distal boundary of the work space, and 3) the ellipses become more isotropic as the hand location is moved to the proximal position. However, the sizes of our stiffness ellipses are considerably smaller than those reported in their results.

Figure 5 (b) also shows the corresponding viscosity ellipses that graphically represent the locus of hand force vectors responding to hand velocity vectors of unit lengths (1 m/s). The major axis of the viscosity ellipse is nearly coaligned with the corresponding stiffness ellipse, i.e., it has a polar arrangement, and that the shapes of the viscosity ellipses become to be thinner near the distal boundary of the work space in the almost same manner as the stiffness ellipses.

4. Spatial Characteristics of Viscoelastic Ellipses

Each ellipse coresponding to the hand stiffness and viscosity represented in the previous chapter can be characterized by three parameters: (1) the size (defined by the ellipse area), (2) the orientation (defined by the counter-clockwise angle from the radial axis of the polar coordinate system to the major axis of the ellipse: see Fig.6), and (3) the shape (defined by the ratio between the lengths of the major and minor axes). Using the elements of the symmetric two-dimensional polar viscoelastic matrix S corresponding to the stiffness or viscosity:
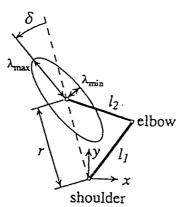
Fig.6 Graphical representation of hand stiffness and viscosity

$$S = \begin{pmatrix} S_{rr} & S_c \\ S_c & S_{\phi\phi} \end{pmatrix}, \quad (3)$$

the size, orientation and shape can be computed as follows [5] and [6]:

$$\lambda_{2,1} = \tfrac{1}{2}[(s_{rr} + s_{\phi\phi}) \pm \sqrt{(s_{rr} + s_{\phi\phi})^2 + 4(s_c^2 - s_{rr}s_{\phi\phi})}\,], \quad (4)$$

$$a = \pi\lambda_1\lambda_2, \quad (5)$$

$$\delta = \tan^{-1}\frac{\lambda_2 - S_{rr}}{S_c} \quad (6)$$

$$b = \frac{\lambda_1}{\lambda_2} \quad (7)$$

where S_{rr} and $S_{\phi\phi}$ represent the viscoelastic components in the radial and polar directions, respectively, and S_c is the coupling term relating to both directions. λ_i denotes the eigenvalue ($\lambda_2 \geq \lambda_1$), and a, δ and b are the size (area), orientation, and shape values, respectively.

4.1 Size of Ellipses

As regards the estimated stiffness and viscosity ellipses in this paper, their spatial variations are consistent with the experimental results of Mussa-Ivaldi et al. [4] and Dolan et al. [6], while the sizes of our ellipses are considerably smaller than theirs, i.e., our postures were maintained with a considerably smaller hand stiffness and viscosity. The difference between the previous experiments and this paper is the way to constrain the hand of the subject to the manipulandum. While the subjects in the setup of [4] and [6] were required to grasp the handle, our subjects didn't need to do so since the molded plastic cast fixing the wrist and the hand was tightly attached to the robot handle.

In order to examine the difference, another plastic cast was used in the experiments. The plastic cast fixed the wrist

joint, but the hand was free, and so the subjects had to grasp the handle in order to keep the hand location. **Figure 7** shows the results in a graphical way, plotting the stiffness and viscosity ellipses in the two cases. The solid and dashed ellipses show the estimated viscoelasticity with and without grasping.

The size, orientation and shape of the ellipses were computed to give a more intuitive interpretation of the difference between the two cases (**Table 2**). It seems that the sizes of both the stiffness and viscosity ellipses are increased by grasping the handle. As pointed out by Gomi et al. [9], a likely explanation of the increase may come from contraction of the muscles caused by grip forces in order to grasp the handle, since there are some multi-joint muscles which act on both the hand and elbow movements.
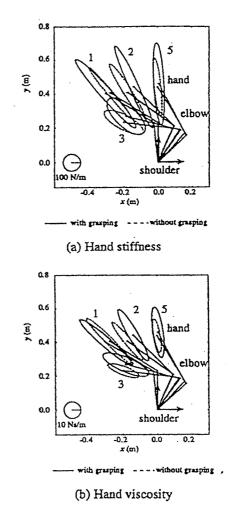

— with grasping – – – without grasping

(a) Hand stiffness

— with grasping – – – without grasping ,

(b) Hand viscosity

Fig.7 The effects of grasping the handle on the estimated stiffness and viscosity ellipses

427

Table 2 Geometrical parameters of estimated stiffness and viscosity ellipses in Fig.7.
Mean values and standard deviations for 10 sets of estimated results are shown.

Grasping force	Hand -location	Stiffness ellipses			Viscosity ellipses		
		Size $[\times 10^4 \ (N/m)^2]$	Orientation [deg.]	Shape [dimensionless]	Size $[(Ns/m)^2]$	Orientation [deg.]	Shape [dimensionless]
without	1	3.85±1.34	4.64±2.52	16.25±11.28	529.59±66.13	10.35±1.64	9.03±0.76
	2	6.23±1.85	8.93±1.96	8.42±1.38	380.11±95.82	15.43±2.00	6.74±0.49
	3	6.95±2.09	22.11±3.23	3.08±0.32	309.05±41.87	28.65±1.54	3.98±0.47
	5	4.10±1.10	5.98±1.81	9.61±2.41	245.80±39.14	10.09±1.06	5.29±0.30
with	1	10.09±2.89	3.07±2.09	8.87±2.64	706.31±99.73	11.91±1.70	7.27±1.30
	2	9.13±2.77	7.00±2.16	10.77±3.28	626.85±75.32	12.10±2.29	6.22±0.51
	3	11.49±2.98	12.18±3.41	2.26±0.26	788.20±93.41	32.32±1.63	3.47±0.32
	5	9.06±1.84	4.08±2.41	8.47±1.20	580.88±50.83	8.712±1.93	4.96±2.09

4.2 Orientation of Ellipses

The major axes of our estimated hand viscoelastic ellipses were approximately oriented toward the subject's shoulder (see Fig.5). In this section, the relationship between the joint viscoelasticity and the orientation of the ellipses is analyzed.

The kinematic relationship between the hand viscoelastic matrix S represented in the polar coordinate system (see eq. (3)) and the joint impedance matrix R can be written as [5]

$$S = P^T J^{-T} R J^{-1} P, \quad (8)$$

where the joint viscoelastic matrix R is defined as a symmetric one:

$$R = \begin{pmatrix} R_{ss} & R_c \\ R_c & R_{ee} \end{pmatrix}. \quad (9)$$

R_{ss} and R_{ee} represent the shoulder and elbow components, respectively, and R_c denotes the coupling component between the shoulder and elbow joints. Also, P and J in (8) are the Jacobian matrices describing differential transformations from polar to Cartesian and from joint to Cartesian velocities, respectively, and given as:

$$P = \frac{1}{r} \begin{pmatrix} l_1\cos\theta_s + l_2\cos(\theta_s + \theta_e) & -l_1\sin\theta_s - l_2\sin(\theta_s + \theta_e) \\ l_1\sin\theta_s + l_2\sin(\theta_s + \theta_e) & l_1\cos\theta_s + l_2\cos(\theta_s + \theta_e) \end{pmatrix} \quad (10)$$

where r is the distance from the shoulder joint to the hand: $r = \sqrt{l_1^2 + l_2^2 + l_1 l_2 \cos\theta_e}$, θ_s and θ_e denote shoulder and elbow joint angles, respectively (see Fig.2) and

$$J = \begin{pmatrix} -l_1\sin\theta_s - l_2\sin(\theta_s + \theta_e) & -l_2\sin(\theta_s + \theta_e) \\ l_1\cos\theta_s + l_2\cos(\theta_s + \theta_e) & l_2\cos(\theta_s + \theta_e) \end{pmatrix}, \quad (11)$$

where l_1 and l_2 are the length of forearm and upper arm, respectively.

Figure 8 shows the relationship among the orientation of the ellipse, δ, the distance parameter, r, and
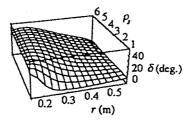
the joint viscoelastic matrix, which is computed by using eqs. (6) and (8). The joint viscoelastic matrix, R, is represented as follows,

$$R = \begin{pmatrix} \rho_s R_c & R_c \\ R_c & \rho_e R_c \end{pmatrix} = R_c \begin{pmatrix} \rho_s & 1 \\ 1 & \rho_e \end{pmatrix}, \quad (12)$$
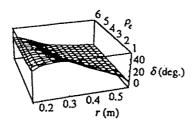
where ρ_s and ρ_e is the ratio of the shoulder and elbow joint components to the coupling one, respectively, and it can be seen that the coupling component R_c is independent of the orientation and shape of the hand impedance ellipse.

In Fig.8 (a), the elbow viscoelasticity ratio ρ_e is fixed to the corresponding mean value of the estimated joint stiffness for 20 different hand locations of the subject ($\rho_e = 3.286$). On the other hand, in Fig.8 (b), the shoulder impedance ratio ρ_s was fixed ($\rho_s = 3.302$). From Fig.8, It can be observed that as the distance r becomes large, i.e., the hand location approaches the distal boundary of the work space, the major axis of the ellipse approaches the radial axis of the polar coordinate system, which is agree with the experimental results shown in the section 3.2.

Then, the orientation values δ of the estimated ellipses shown in Fig.5 are plotted with respect to the distance r in Fig.9. Fig.9 (a) and (b) are corresponding to the hand stiffness ellipses and the viscosity ellipses, respectively, and the solid lines in both figures show the computed orientation δ using eqs. (6) and (8) with the mean values of the estimated joint impedance ratio ρ_s and ρ_e for 20 different hand locations of the subject: $\rho_s = 3.302$ and $\rho_e = 3.286$ for stiffness (Fig.9 (a)), and $\rho_s = 3.153$ and $\rho_e = 2.182$ for viscosity (Fig.9 (b)). While the variation of the experimental data is a bit large, the computed orientation in both cases (the solid lines) well capture with the feature of the experimental results. Also it can be seen from the figure that the orientation values of the hand stiffness ellipses are smaller than the ones of the viscosity ellipses.
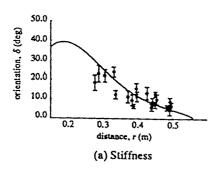
(a) Relationship among the orientaion δ, the shoulder joint impedance ratio ρ_s, and the distance r, where the constant elbow joint impedance ratio is used (ρ_e =3.286).

(b) Relationship among the orientaion δ, the elbow joint impedance ratio ρ_e, and the distance r, where the constant shoulder joint impedance ratio is used (ρ_s =3.302).
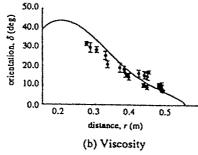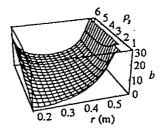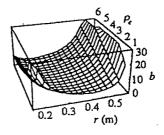
Fig.8 Computed orientation of the hand impedance ellipses
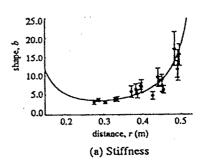

(a) Relationship among the shape b, the shoulder joint impedance ratio ρ_s, and the distance r, where the constant elbow joint impedance ratio is used (ρ_e =3.286).

(b) Relationship among the shape b, the elbow joint impedance ratio ρ_e, and the distance r, where the constant shoulder joint impedance ratio is used (ρ_s =3.302).

Fig.10 Computed shape of the hand impedance ellipses

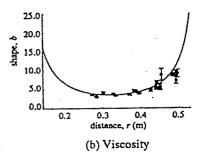
(a) Stiffness

(b) Viscosity

Fig.9 Comparison between computed (solid lines) and estimated orientation of the ellipses

(a) Stiffness

(b) Viscosity

Fig.11 Comparison between computed (solid lines) and estimated shape of the ellipses

429

4.3 Shape of Ellipses

Figure 10 shows the relationship among the shape of the ellipse, b, the distance parameter, r, and the joint viscoelastic ratio ρ_s and ρ_e, which is computed by using eqs. (7) and (8). In Fig.10 (a) and (b), one of the elbow and shoulder joint ratio, ρ_e or ρ_s is fixed to the same mean value as Fig.8. The shape of the ellipse becomes to be thinner, as the hand approaches more distal position, and that the variation of the joint viscoelaticity ratio has less effects to the change of the shape parameter.

Figure 11 shows the estimated shape parameter in our experiments, where Fig.11 (a) and (b) are corresponding to the hand stiffness ellipses and the viscosity ellipses, respectively, and the solid lines in both figures show the computed shape parameter b with the fixed joint viscoelastic ratio in the same way as Fig.9. The experimental results well agree with the computed one. The kinematic factor of the human arm plays a more significant role in determining the spatial characteristics of the hand stiffness and viscosity than the variations of the joint viscoelasticity under our experimental condition.

5. Conclusion

The purpose of this paper was to investigate the spatial characteristics of the hand impedance in multi-joint movements during maintaining the posture. The main results of our experiments can be summarized as follows: 1) spatial variations of the estimated hand impedance ellipses (stiffness, viscosity, inertia) approximately agreed with the experimental results of other researchers [4] - [6], 2) the human hand inertia characteristics can be explained from basic biomechanics of the passive inertial effects, 3) the grip force of the subject increases the size of the stiffness and viscosity ellipses, and 4) spatial features of the orientation and the shape characteristics of the stiffness and viscosity ellipses are mostly explained from the kinematics point of view of the human arm.

Further research will be directed to make clear contributions of several muscles such as single-joint muscles and multiple-joint muscles to the spatial characteristics of the hand impedance ellipse.

Acknowledgments

References

[1] Abul-Haj, C.J., Hogan, N.: Functional assessment of control systems for cybernetics elbow prostheses, IEEE Trans. Biomed. Eng., BME-37, 11, 1025-1036 (1990).

[2] Kazerooni, H. : Human robot interaction via the transfer of power and information signals. IEEE Transaction on System, Man and Cybernetics, 20, 2, 450-463 (1990).

[3] Kosuge, K., Fujisawa, Y., Fukuda, T. : Control of mechanical system with man-machine interaction. Proc of the IEEE/RSJ International Conference on Intelligent Robots and Systems vol.1, 87-92 (1992).

[4] Mussa-Ivaldi, F.A., Hogan, N., Bizzi, E. : Neural, mechanical and geometrical factors subserving arm posture in humans. Journal of Neuroscience 5, 10, 2732-2743 (1985).

[5] Flash, T., Mussa-Ivaldi, F.A.: Human arm stiffness characteristics during maintenance of posture. Experimental Brain Research 82, 315-326 (1990).

[6] Dolan, J.M., Friedman, M.B., Nagurka, M.L.: Dynamic and loaded impedance components in the maintenance of human arm posture. IEEE Transaction on System, Man, and Cybernetics, 23, 3, 698-709 (1993).

[7] Tsuji, T., Goto, K., Ito, K., Nagamachi, M.: Estimation of Human Hand Impedance During Maintenance of Posture. Trans. of the Society of Instrument and Control Engineers, 30, 3, 319-328 (1994), in Japanese.

[8] Winter, D.A.: Biomechanics of human movement. A Willy-Interscience Publication (1979).

[9] Gomi, H., Koike, Y., Kawato, M.: Human hand stiffness during discrete point-to-point multi-joint movement. Proceedings of the Annual International Conference of the IEEE Engineering in Medicine and Biology Society, 1628-1629 (1992).